Meteoritics & Planetary Science 39, Nr 11, 1839–1848 (2004)
Abstract available online at http://meteoritics.org

Pressure effects on martian crustal magnetization near large impact basins

Gunther KLETETSCHKA,[1, 2, 3*] John E. P. CONNERNEY,[3] Norman F. NESS,[4] and Mario H. ACUÑA[3]

[1]Department of Physics, Catholic University of America, Washington D.C., USA
[2]Institute of Geology, Academy of Sciences, Prague, Czech Republic
[3]NASA Goddard Space Flight Center, Greenbelt, Maryland, USA
[4]Bartol Research Institute, University of Delaware, Newark, Delaware, USA
*Corresponding author. E-mail: gunther.kletetschka@gsfc.nasa.gov

(Received 3 February 2004; revision accepted 25 June 2004)

Abstract–Martian crust endured several large meteoroid impacts subsequent to the demise of an early global magnetic field. Shock pressures associated with these impacts demagnetized parts of the crust, to an extent determined by shock resistance of magnetic materials in the crust. Impacts that form large basins generate pressures in excess of 1 GPa within a few crater radii of their impact sites. Crustal materials near the surface experience significantly reduced impact pressure, which varies with depth and distance from the impact point. We present new demagnetization experiments on magnetite (Fe_3O_4), hematite (α-Fe_2O_3), and titanohematite ($Fe_{2-x}Ti_xO_3$ where $x < 0.2$). Our measurements show that pressures of ~1 GPa are sufficient to partially demagnetize all of these minerals. The efficiency of demagnetization by impact pressure is proportional to the logarithm of the minerals' magnetic coercivity. The impact pressure magnetic response from exsolved titanohematite samples is consistent with the magnetization decay near Prometheus impact basin and may point to an oxidized igneous rock in Terra Sirenum region at the time of acquisition of magnetic remanence. The remaining magnetic anomalies near large impact basins suggest moderate crustal coercivity. These anomalies point to titanomagnetite as a magnetic carrier and more reduced condition during crustal formation.

INTRODUCTION

Analyses of martian meteorites and data from Mars Global Surveyor (MGS) have advanced our knowledge of the chemistry and the structure of martian crust and mantle (Zuber 2001). However, many fundamental questions remain to be answered. Among the unexplained problems is the nature of the highly magnetized crustal materials. Crustal magnetization on Mars is at least an order of magnitude greater than on Earth, requiring large volumes of highly magnetized material in Mars' crust (Connerney et al. 1999; Voorhies et al. 2002). The source bodies may be quite thick, perhaps >50 km, and deep seated (≤100 km) (Arkani-Hamed 2002; Nimmo and Gilmore 2001). However, the thickness, magnetization intensity, and source depth are poorly constrained observationally (Connerney et al. 2004).

The 4-Gyr-old (±0.1) martian meteorite ALH 84001 is at present the oldest well-documented sample with remanent magnetization in our solar system (Weiss et al. 2002a, 2002b). Crustal remanence on Mars was likely acquired before the end of the heavy bombardment (Acuña et al. 1999), as evidenced by the lack of magnetization in the centers of impact basins. The shock wave generated by an impact produces high pressures that penetrate and demagnetize the crust well beyond the crater rim (Halekas et al. 2002). If a large ambient magnetic field is present during the impact, the penetrating shock wave can induce a shock remanent magnetization (SRM) in low coercivity minerals (Cisowski and Fuller 1978).

Impact sites are also sources of massive volumes of impact melt which upon cooling would carry magnetic particles. These magnetic minerals would have a strong magnetic remanence if a significant global magnetic field were present when they cooled below their blocking temperatures. The absence of magnetic anomalies over these basins suggests that the cooling occurred most likely in the absence of a global magnetic field.

IMPACT MODEL

We assume that portions of martian crust were demagnetized by shock associated with large impacts and in the absence of a dynamo. The temperatures achieved near an impact site will also demagnetize the crust (Mohit and Arkani-Hamed 2004). While analyzing magnetic anomalies

Table 1. Crater data: crater locations are determined by latitude and W longitude. CD/I is a crater diameter and depth to 1 GPa interference zone at CD distance, ID is an impactor's diameter calculated from CD using the impact scaling code developed by H. J. Melosh, available at http://www.lpl.arizona.edu/tekton/crater.html. PD1, PD2, and PD5 are the distances of peak pressure (1, 2, and 5 GPa) isolines estimated from the momentum conservation equations.

Crater	Latitude (°)	Longitude (°)	CD/I (km)	ID (km)	PD1 (km)	PD2 (km)	PD5 (km)
Hellas	–42	294	1520/6.7	520	9440	6530	4030
Isidis	13	273	1200/5.2	380	6970	4820	2970
Argyre	–50	42	1000/4.3	300	5520	3820	2360
Prometheus	–84	266	860/3.6	250	4550	3150	1940

near the large impact basins, we have applied models for shock pressure propagation from the point of impact on Mars (Hood et al. 2003). We analyze impact pressures in four large impact basins of Mars: Prometheus (Milkovich et al. 2002; Schenk and Moore 2000; Tanaka and Scott 1987), Argyre, Hellas, and Isidis (Tanaka et al. 1986).

The Hugoniot Equation

$$P(r) = \rho_{ot}[C_t + S_t u_0 (r_0/r)^{1.87}] u_0 (r_0/r)^{1.87} \quad (1)$$

The Hugoniot equation approximates the shock pressure decay $P(r)$ with radial distance r perpendicular to the surface, directly below the impact point, from an empirical determination of particle velocity decay (Melosh 1989). Here, ρ_{ot} is the unshocked target mass density, C_t and S_t are empirically determined shock parameters (Melosh 1989), and u_0 is the initial particle velocity at distance r_0 from the impact point. Therefore, r_0 indicates the radius of the impactor. The radius of the impactor is estimated by the π-scaling law from the knowledge of the radii of transient basin diameters (Schmidt and Housen 1987). The scaling laws apply to the formation of simple and complex craters, and are less appropriate for the basin-forming regime where they will likely underestimate the size of the impact projectile.

Assuming that the transient crater rim coincides with the inner topographic boundaries, as reported for Chicxulub (Morgan et al. 1997), one obtains estimates of impactor diameters from the Mars Orbiter Laser Altimeter (MOLA) topography data (Smith et al. 1999) (see Table 1) for these basins using the planar impact approximation (Ahrens and O'Keefe 1977).[1] Solving Equation 1 for the radius r of the maximum pressure delivered by impact gives:

$$r = r_0 \left(\frac{1}{u_0} \sqrt{\frac{1}{4}\left(\frac{C_t}{S_t}\right)^2 + \frac{P}{\rho_{ot} S_t}} - \frac{1}{2}\frac{C_t}{S_t} \right)^{-\frac{1}{1.87}} \quad (2)$$

[1]The impact code was developed by H. J. Melosh and is available at http://www.lpl.arizona.edu/tekton/crater.html. Input parameters used: 2900 kg/m^3 for impactor and target density (gabbroic anorthosite composition); 3.72 m/s^2 for the gravity acceleration; 45° for the most probable impact angle. Planar approximations give a peak particle velocity of 7.5 km/s for a gabbroic anorthosite impactor impacting on a gabbroic anorthosite target at 15 km/s.

Isobars for 1, 2, and 5 GPa pressures are plotted in Fig. 1 for the large impact basins of Mars, Prometheus, Argyre, Hellas, and Isidis. For crater location and calculated pressure diameters see Table 1. However, the pressure hemisphere does not extend to the surface because the pressure on the surface is by definition zero. The boundary condition (zero pressure) on the surface is accomplished by a rarefaction wave, equal in strength but opposite in sign to the shock wave, which propagates downward from the surface as soon as the shock wave arrives. The sum of the pressure in shock and rarefaction waves is always zero on the free surface and interference between the two waves occurs below the surface (see Fig. 5.7, Melosh 1989). The onset of the maximum interference pressure is a complex function of time (Melosh 1989), which we need not be concerned with. The maximum pressure experienced by the rock inside the interference zone increases more or less linearly with depth (see Figs. 5.7 and 5.8 in Melosh 1989) until it reaches the maximum pressure predicted (see also Table 1). Therefore, the pressures estimated from the Hugoniot equations (Hood et al. 2003) are only valid at the bottom of the interference zone, the depth z_s that can be estimated (Melosh 1989) from:

$$z_s = \frac{U_t \tau_r}{2} \sqrt{1 + \frac{s^2}{d_{eq}^2 + \left(\frac{U_t \tau_r}{2}\right)^2}} \quad (3)$$

Here, s is the horizontal distance across the surface from the impact site to the position where the depth of the interference zone is evaluated, the product $U_t \tau_r$ is the width of the rising portion of the shock wave that is roughly equal to the projectile's radius, and d_{eq} is the equivalent impact center depth. We estimate the depth at which the rock experienced pressures exceeding 1 GPa (Fig. 2) allowing for approximately linear decrease in pressure toward the surface.

Observations

The identification of crustal magnetic signatures on Mars with specific geological/topographic features is difficult and controversial. As yet, there is no clear association between the magnetism of the martian crust and surface morphology beyond the association with topography evidenced in the

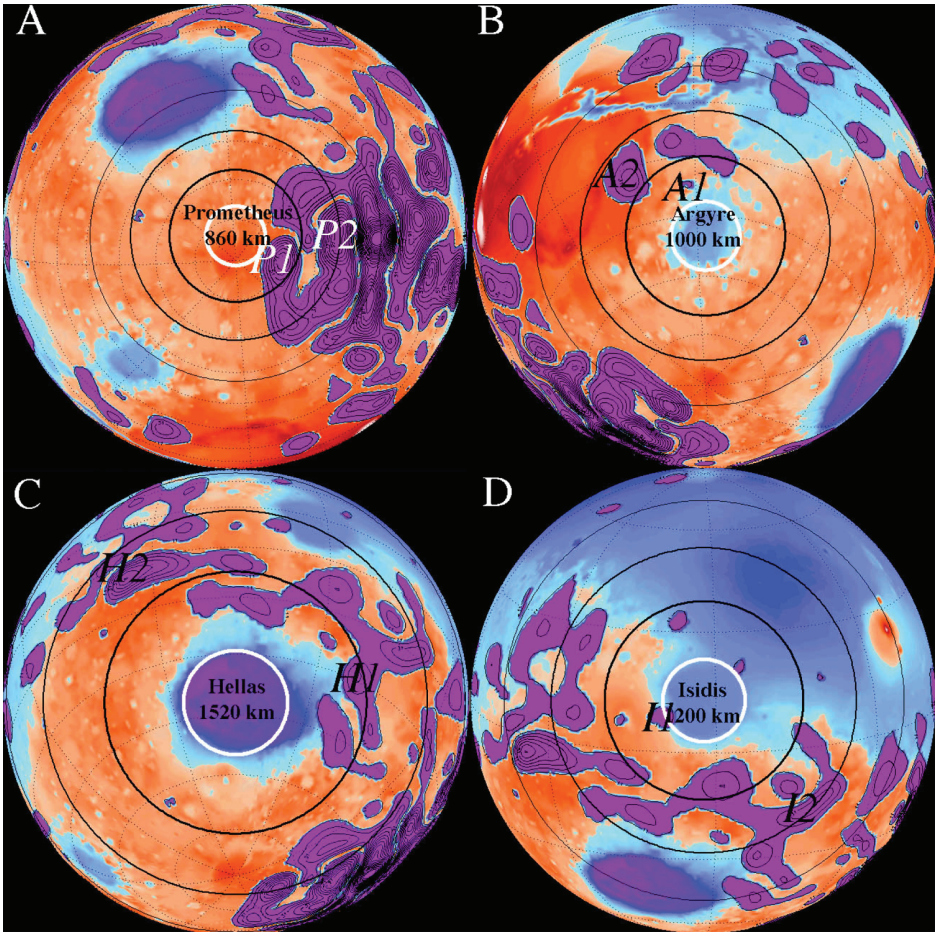

Fig. 1. MGS MOLA topographic maps (dark red is the highest and dark blue is the lowest altitude) compared with MGS magnetic maps across large impact basins: a) Prometheus; b) Argyre; c) Hellas; and d) Isidis. The purple color indicates the absolute values of radial magnetic signature exceeding 10 nT at night side and 400 km satellite altitude. The contour lines have a contour interval of 10 nT. The heavy white circle is the crater diameter. The circles of increasing diameters indicate the peak pressure exceeding 5, 2, and 1 GPa, respectively, during the impacts (estimated analytically, see text).

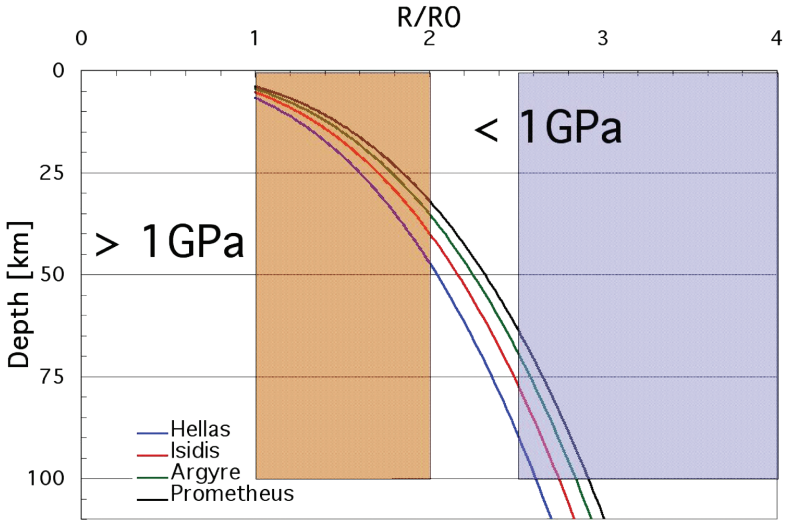

Fig. 2. Plot of the distance from the center of impact versus depth where the maximum impact pressure exposure exceeds 1 GPa. The hypothetical source of magnetic anomalies, the majority of which experienced pressures exceeding 1 GPa, is shown in brown and the source affected by impact pressures of less than 1 GPa is shown in light blue.

crustal dichotomy and the largest impact basins (Acuña et al. 1999) and broad spatial correlation with the martian valley networks (Harrison and Grimm 2002). In this work, we examine crustal regions on Mars that contain magnetic sources and are also close to the center of a large impact basin. For our analysis, we work with contours of the radial magnetic field measured at the altitude of 400 km (Connerney et al. 2001; see Fig. 1). A minimum contour value of 10 nT was chosen to eliminate spurious field of external origin.

Magnetic maps across major impact basins on Mars show a clear absence of magnetic field toward the centers of these basins (Fig. 1). However, the occurrence of magnetization close to the impact basin's center indicates the presence of magnetic minerals capable of retaining magnetization despite the shock event. Most of the work on pressure demagnetization shows that demagnetization effects increase with the magnetic coercivity (Hc) of the magnetic carrier (impact experiments: Cisowski and Fuller 1978; Nagata 1971; Pohl et al. 1975; static experiments: Rochette et al. 2003; observational compendium: Pilkington and Grieve 1992).

EXPERIMENTS

We have measured the saturation remanent magnetization and natural remanent magnetization (NRM) of magnetic minerals (measured by superconducting rock magnetometer, 2G Inc.), subjected these minerals to a low-level impact pressure (1 GPa) in a weak magnetic field (≈100 nT), and re-measured the magnetic remanence after the impact. The magnetic inclination of samples is in respect to the vertical impact direction. For example, 0° of the NRM inclination indicates that the magnetization vector of the specimen is perpendicular to the impact's direction (see Table 3). We have chosen the most common candidate magnetic minerals that can contribute appreciably to magnetic sources and are likely to be present within the deep martian crust. These are multidomain (MD) magnetite, single (SD)/pseudosingle domain magnetite, MD hematite, and exsolved titanohematite. Multidomain hematite and magnetite samples were characterized (Kletetschka et al. 2000a) by hysteresis properties, microprobe, X-ray diffraction, and Morin and Verwey transitions (Kletetschka and Wasilewski 2002), respectively. Single domain magnetite is naturally dispersed in green spinel and was characterized by hysteresis properties, microprobe, and Verwey transition (Kletetschka 1998). Finally, titanohematite (sample w6b has 9% of dissolved ilmenite component (Kletetschka et al. 2002) with exsolved lamellae of ferrian ilmenite was characterized by hysteresis properties, microprobe, and reflected light microscopy (Kletetschka 1998).

Amplitudes of the NRM for exsolution of SD magnetite within a spinel varied within the range of 0.03–0.70 Am^2/kg; 0.02–0.04 Am^2/kg for MD magnetite; 0.05–0.45 Am^2/kg for MD hematite; and 0.1–0.5 Am^2/kg for titanohematite. The nature of the NRM in all of these samples, except the MD magnetite, is most likely the chemical remanent magnetization where the magnetic phase formed as exsolution or chemical precipitation below the Curie temperature of the mineral. These minerals have only one magnetic component as evidenced by the alternating field (AF) demagnetization of the parent rock (Kletetschka 1998; Kletetschka and Stout 1998). We acquired one thernal remanent magnetization (TRM) laboratory component at 50,000 nT in MD magnetite (large single crystal samples).

Samples have a broad spectrum of magnetic coercivity and, thus, were well chosen to show the effects of coercivity on impact pressure demagnetization reported previously (Cisowski and Fuller 1978; Nagata 1971; Pilkington and Grieve 1992; Pohl et al. 1975). Multidomain hematite has higher magnetic coercivity (Hc = 13 mT) than MD magnetite (Hc = 1.8 mT) due to a low demagnetizing energy and, thus, the large amount of pinning energy holding the domain walls in place (Kletetschka et al. 2000c). The SD magnetite has larger coercivity (Hc = 19 mT) than MD magnetite due to absence of domain walls. The magnetic mineral with the largest coercivity (Hc ~260 mT) is exsolved titanohematite in which the coercivity is increased by exsolution processes (Kletetschka et al. 2002) and/or by lamellar magnetism (Robinson et al. 2002). For all of the minerals studied, the rigidity (shear) modulus was comparable, e.g., 91.2 GPa for magnetite, 91.0 GPa for hematite, and 108.5 GPa for spinel (see Bass 1995).

We used a magnetically shielded target area (<100 nT, μ-metal-shielded space) at room temperature and pressure during impact experiments (Fig. 3b). We positioned an aluminum plate 1.5 cm-thick and 7 cm in diameter beneath the target and atop a 10 kg lead brick resting on foam shock absorbers. Magnetic minerals were shaped into rectangular fragments with 10 ± 3 mm^2 impact area and 1.0 ± 0.5 mm thick. Samples were positioned in the center of a circular glass slide (25.4 mm in diameter and 1.5 mm thick) and surrounded by a thin strip of non-magnetic play dough to preserve the glass assembly after the impact (Fig. 3c left). A 1 kg standard mass was used for an impact projectile. A second glass slide of identical shape was taped to the front impact area of the impactor (Fig. 3c middle). Guided by a non-magnetic ventilated impact shaft, the impactor was dropped from the height of 1 m, onto a magnetically shielded sample area (Fig. 3c right) to achieve the impact pressure of ~1 GPa. The samples penetrated and shattered the glass slide, coming to rest between the two glass slides (Fig. 3c left). The pressure experienced by the sample is estimated using:

$$P = \frac{mg\frac{S}{S'}}{A} \quad (4)$$

where m is the mass of the impactor (1 kg), g is gravitational acceleration (9.81 m/s^2), S is the accelerating distance of the impactor (1.00 m), S' is the decelerating distance (equal to the

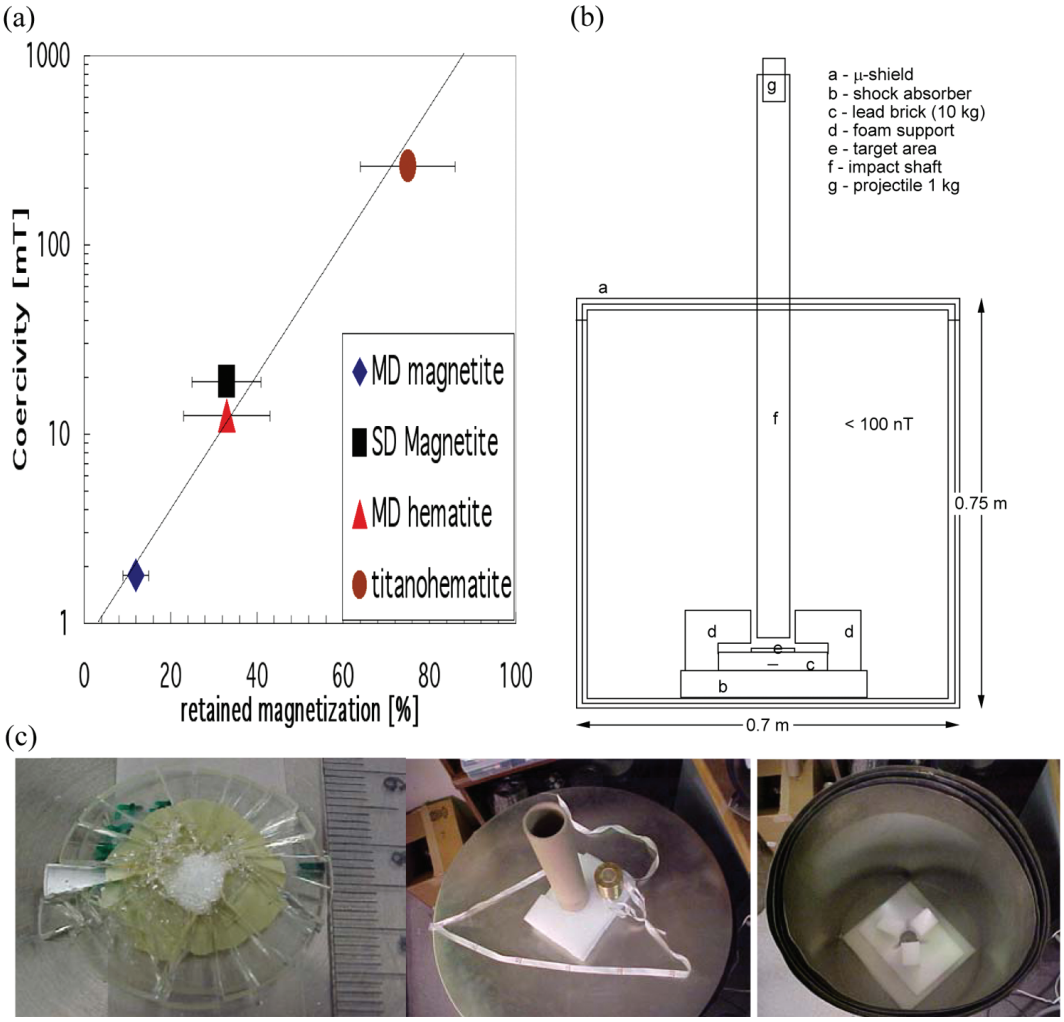

Fig. 3. a) The magnetic coercivity of minerals is plotted against measurements of magnetic response to ~0.5–2.0 GPa shock pressure for various minerals. The error bars are based on 5 samples of MD magnetite, 3 samples of SD magnetite, 18 samples of MD hematite, and 16 samples of titanohematite with ilmenite exsolution; b) a schematic of the impact apparatus to scale; c) geometry of the experiment: left-the sample after the impact of the 1 kg weight is trapped between the pair of two glass slides stuck together by a small amount of play dough. The samples were ~3 mm in diameter; middle-the impact shaft directs the brass 1 kg weight to the sample impact area. The impact shaft is lifted above the sample area by about 4 cm to allow the air mass in front of the projectile to escape during the free fall; right-the sample chamber is equipped with a 3-layer m-shielded chamber with the background noise of 100 nT. The circular glass slide rests on aluminum cylinder on top of the lead brick suspended on shock absorbers.

samples' thickness; 1.0 ± 0.5 mm), and A is the impact area (10 ± 3 mm^2). Given these uncertainties, the resulting impact pressure was between 0.5 GPa and 2 GPa. Air friction was neglected. The play dough and tape held the sample inside the pair of glass slides after impact. The magnetic remanence measurements were performed directly on the post-impact glass assembly containing the samples. Stress concentrations associated with the penetration process may have slightly increased the peak pressure experienced by the sample. Sample diameters are about 3 mm, i.e., about the same thickness as a pair of two glass slides after the impact. If the sample had been slightly thinner, the peak pressure would have been lower than assumed. These considerations result in fairly large uncertainties in the estimated peak pressures.

RESULTS

The percentage of initial remanent magnetization (both natural and saturated) that remained after impact (~1 GPa), averaged over many samples, groups by mineralogy (Fig. 3; Table 3). The efficiency of demagnetization was insensitive to the direction of the original magnetization. Different minerals endured the impact with different resistance to demagnetization. MD magnetite retained the least amount of magnetization (12 ± 3%) and had the lowest magnetic coercivity (1.8 mT). Both moderate coercivity minerals hematite and magnetite (13 mT and 19 mT for MD hematite and SD magnetite) retained 33 ± 10%, and 33 ± 8%, respectively. Titanohematite with exsolved lamellae had the

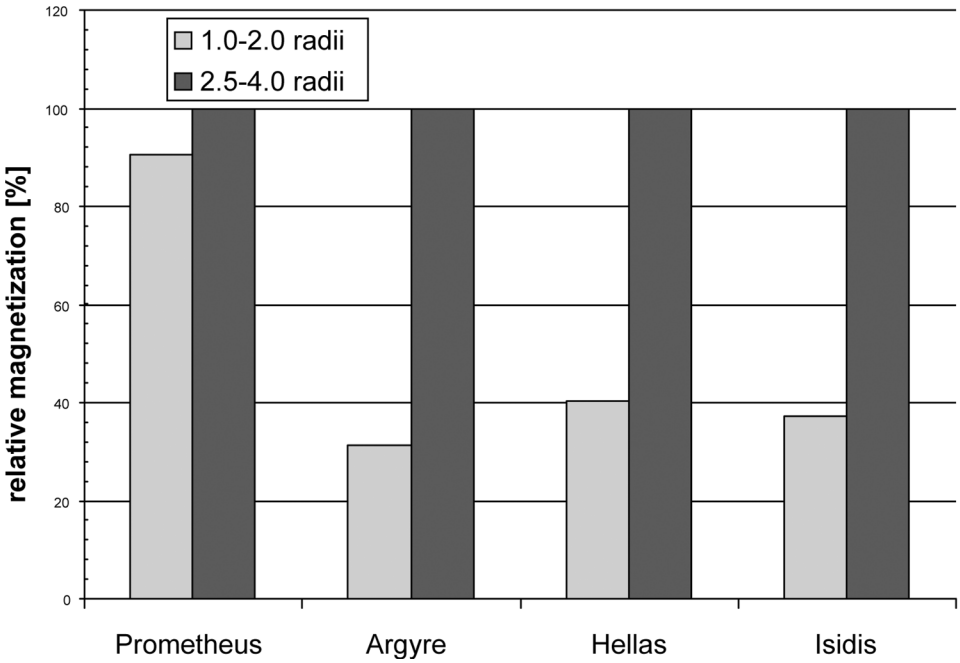

Fig. 4. The relative magnetization near large impact basins deduced from large-scale magnetic anomalies (Fig. 1; Table 2) that occur within the specified distance (1.0–2.0 and 2.5–4.0 radii) from the centers of the large craters.

largest coercivity (260 mT) and retained 75 ± 11% of its original remanent magnetization. The correlation between coercivity and pressure demagnetization, illustrated in Fig. 3a, indicates a proportionality relationship of $M_{\%} \propto \log(Hc)$, where $M_{\%}$ is the percentage of remanent magnetization retained post-impact. This dependence is supported by numerous experimental observations (Cisowski and Fuller 1978; Nagata 1971; Pilkington and Grieve 1992; Pohl et al. 1975). Our experiments on magnetic MD and SD magnetite are consistent with recent diamond anvil static pressure measurements on MD and SD magnetite (Gilder et al. 2002) where the saturation magnetization of both MD and SD magnetite decreased by more than 50% after application of 3 GPa static pressure. Recent work (Rochette et al. 2003) indicates that pyrrhotite, another common rock-forming mineral, completely demagnetizes at 3 GPa at room temperature and retains less than 50% of its original magnetization between 1 and 2 GPa.

Our shock demagnetization data are compared with the major impact basins on Mars (Fig. 1). Based on our modeling (Figs. 1 and 2), and assuming that the magnetic sources are not deeper than 100 km, only the regions within ~2.5 crater radii of the impact basins can be significantly modified by the impact pressure. Most of the anomaly sources reside at depths less than 100 km (Arkani-Hamed 2002; Connerney et al. 1999; Nimmo and Gilmore 2001; Voorhies et al. 2002).

Figure 2 shows that the pressure exceeds 1 GPa in most of the magnetic source volumes occurring at the distances of <2 crater radii and shallower than 100 km. However, the magnetic source volumes that are further from their impact basin (within 2.5–4.0 radii) should be affected by pressures not exceeding 1 GPa (see Fig. 2). For lack of more detailed information, we assume that the intensity of magnetization in the crust scales linearly with the amplitude of the magnetic field measured above at satellite altitude. This would be the case, for example, if the field were due to a distribution of randomly oriented dipole sources in the crust. This estimate neglects potentially significant details of the source distribution, for example, the thickness of the magnetized layer, systematic variation in source geometry, and/or magnetization direction. We regard this estimate with caution and proceed with the assumption that this crustal magnetization can be crudely correlated to our experimental magnetic response of minerals (Fig. 3).

DISCUSSION

Figure 4 and Table 2 illustrates how maxima of the magnetic anomalies, one located within 1.0–2.0 crater radii and the second one within 2.5–4.0 crater radii (see Fig. 1), decrease with the proximity to a large impact basins. Beyond ~2.5 crater radii, the impact pressure does not exceed 1 GPa (Fig. 2) and this crustal source volume is not significantly affected by the impact. The purpose of this study is to estimate the relative demagnetization of the source volume inside the near region (1.0–2.0 radii) that relates to an observable magnetic anomaly. We locate the largest anomaly in the near region and divide it by the largest magnetic anomaly in the far region (2.5–4.0 radii). This procedure neglects important characteristics of source distribution and

Table 2. Magnetic anomalies (radial component) near large impact basins.

Magnetic anomaly	Magnitude (nT)	Distance (R/R0)	Latitude/ longitude
P1	95.9	1.83	–78.2/175.1
P2	105.0	3.62	–63.6/180.5
A1	15.0	1.61	–37.1/48.1
A2	48.5	2.76	–33.7/64.8
H1	33.2	1.97	–16.9/289.8
H2	84.3	3.54	–4.6/323.8
I1	16.8	1.75	9.2/285.7
I2	41.0	3.95	–15.5/244.5

only crudely indicates the demagnetization effect of the original crustal magnetization. This decrease in crustal magnetization near the impact basins can then be related to our experimentally derived response to an impact pressure in terms of magnetic coercivity (Fig. 3). The 60–70% decrease in magnetization (Fig. 4) for Hellas, Argyre, and Isidis impact basins suggest the magnetic anomalies near these basins are caused by magnetic mineral with moderate magnetic coercivity of ~10 mT (e.g., SD magnetite). A 10% decrease in magnetization observed for Prometheus (Fig. 4) can only be explained by magnetic minerals that have large magnetic coercivity (~1000 mT). This large value of magnetic coercivity rules out magnetite as a magnetic carrier.

Prometheus basin is the only large impact basin near the highly magnetized rocks in Terra Sirenum containing compact and very intense magnetic anomalies (southern hemisphere between 140–210° W longitude). It is suggested that magnetic anomalies within Terra Sirenum have different nature of its magnetic source due to contrasting coercivity requirement near this impact basin. Prometheus basin toward Hellas and Argyre has very little of the magnetic signature. This suggests that Prometheus impact is along the boundary where the nature of the crustal magnetic source changes from a less stable to a stable and intense magnetic sources (Fig. 1a).

Magnetic signatures around impact basins suggest the existence of three different types of magnetic sources in the crust. The first type contains magnetic mineral of intense remanence and large coercivity (e.g., titanohematite) and the distribution is suggested by the occurrence of large magnetic anomalies (Fig. 1). The second type of magnetic crust contains magnetic minerals with moderate magnetic coercivity (e.g., SD magnetite) and is characterized by moderate magnetic anomalies. The third type has little or no magnetic signature and is either younger than the pre-existing dynamo or the magnetic carriers were replaced after the dynamo shut down. It is also conceivable that the magnetic source may have very small magnetic coercivity (MD magnetite) and, thus, any magnetization it once had was unstable and decayed to a negligible value as a result of elevated temperatures in the deep crust.

The contrasting behavior of magnetic anomalies around Prometheus was in fact well supported by evidence in the work of Langlais et al. (2004; Fig. 6), though not pointed out in the text. Few magnetic minerals have large coercivity needed to explain the magnetic decay indicated near Prometheus basin. To preserve large coercivity, in general magnetic minerals have large magnetic anisotropy allowing an acquisition of magnetization only in certain directions. The most common rock-forming magnetic minerals of this nature are (titano-) hematite and pyrrhotite.

The magnetization of hematite and pyrrhotite in their pure form changes with grain size (Kletetschka et al. 2003). The maximum possible TRM of large grains of hematite and pyrrhotite is a little over 1,000 A/m. Since both hematite and pyrrhotite can acquire strong magnetizations while in large grain size, they could be part of large iron formations that may have formed due to hydrothermal alteration early in Mars' history. In such cases, the concentration of hematite and/or pyrrhotite can exceed 50% by volume and the intensity of magnetization of the bulk material can reach 500 A/m (Kletetschka et al. 2000b).

The presence of hematite in lower crustal martian rocks would imply high oxidation levels. The occurrence of hematite bearing lower crustal rocks on Earth is commonly attributed to the orogenic recycling of oxidized surface material (Frost 1991)—a process for which there is no clear evidence on Mars so far. Pyrrhotite has been detected in the SNC meteorites and suggests a possibility of large hydrothermal flows accumulating this mineral in a massive form.

Titanohematite has both impact resistant remanence and sufficient magnetic intensity. Titanohematite and/or hematite occurs frequently in the oxidized crust of the Earth including the lower crustal rocks (Kletetschka and Stout 1998; Kletetschka et al. 2002; McEnroe et al. 2001a, 2001b). Crustal rocks can be also oxidized later as a result of hydrothermal activity producing alteration zones with gradual decomposition of primary magnetite to hematite (Just et al. 2002) (martitization). Post-magmatic pervasive alteration can take place during the early cooling history of the rock. This alteration is associated with retrograde P-T conditions and different paragenesis implicating several episodes of fluid circulation. With a decrease of temperature, oxygen fugacity increases. The oxidation of the magnetite can occur with a later stage of the pervasive alteration when biotite chloritizes within a temperature interval between 180–200 °C and pressures between 0.2–0.3 GPa (Jacquemont 2002). Due to the low magnetic intensity of the altered minerals (Just 2003, personal communication), and because this kind of alteration produces pure hematite as opposed to titanohematite exsolution, it is probably not a viable explanation for generating very intense magnetic anomalies on Mars.

Another potential magnetic source can be a metasedimentary high-grade rock which can contain intensely magnetic titanohematite (Kletetschka and Stout 1998;

Table 3. Impact magnetic data on various minerals: NRM = natural remanent magnetization; SIRM = saturation remanent magnetization; I = magnetic inclination (a value of 0° inclination is perpendicular to the impact direction); D = magnetic declination.

Sample name	Condition	M (Am^2/kg)	I (°)	D (°)	Sample name	Condition	M (Am^2/kg)	I (°)	D (°)
MD magnetite					SD magnetite				
90lp12c1	NRM	0.0275	–22	257	w6sp2	SIRM	1.2489	–17	44
	impact	0.0036	–27	258		impact	0.3706	–31	45
90lp12c2	NRM	0.0331	8	21	w6sp3	NRM	0.7379	72	355
	impact	0.0049	–35	41		impact	0.3116	50	45
90lp12c3	NRM	0.0234	–82	257	w6sp4	NRM	0.4247	9	359
	impact	0.0016	–87	258		impact	0.1191	–3	10
90lp12c4	NRM	0.0421	45	21					
	impact	0.0051	–35	41					
90lp12c5	NRM	0.0366	–52	257	Exsolved titanohematite				
	impact	0.0046	24	258	w6s1	NRM	0.1378	–18	56
MD hematite						impact	0.1032	–11	61
115249s1	SIRM	0.3224	5	70	w6s2	NRM	0.1206	–14	62
	impact	0.1359	2	80		impact	0.1155	–11	68
c6103c1	NRM	0.1535	–17	164	w6s3	SIRM	0.4095	–11	327
	impact	0.0441	–16	180		impact	0.1803	–8	340
c6103c2	NRM	0.0676	–46	80	w6s4	NRM	0.0996	3	120
	impact	0.0282	–20	29		impact	0.0123	–9	198
c6103c3	NRM	0.1379	–34	304	w6s5	NRM	0.0850	–42	299
	impact	0.0452	–23	308		impact	0.0594	–43	288
orrs1	NRM	0.2335	–58	104	w6s6	NRM2	0.0344	–59	159
	impact	0.0994	–11	97		impact	0.0317	–32	148
orrs2	NRM	0.3214	–48	273	w6s7	NRM	0.1216	84	324
	impact	0.0783	–25	261		impact	0.1061	66	290
orrs3	NRM	0.1827	–16	79	w6s8	NRM	0.0917	–39	146
	impact	0.0419	–9	85		impact	0.0526	–28	140
orrs4	NRM	0.1493	10	92	w6s9	NRM	0.0709	–30	255
	impact	0.0611	37	92		impact	0.0426	–15	240
orrs5	NRM	0.1380	–19	91	w6s10	NRM	0.0413	–17	206
	impact	0.0309	5	93		impact	0.0282	–16	190
orrs6	NRM	0.2312	–70	224	w6s11	SIRM	0.1272	–14	2
	impact	0.0237	–30	83		impact	0.1027	–11	359
orrs7	NRM	0.4065	48	272	w6s12	NRM	0.0555	10	202
	impact	0.1012	2	272		impact	0.0430	12	241
orrs8	NRM	0.2977	80	116	w6s13	NRM	0.0488	–1	141
	impact	0.0510	25	91		impact	0.0389	6	132
ors1	SIRM	0.3784	8	95	w6dm1	SIRM	0.1325	48	322
	impact	0.1616	4	89		impact	0.1107	48	322
ors2	SIRM	0.4441	0	91	w6dm2	SIRM	0.1370	7	16
	impact	0.1988	3	86		impact	0.0929	18	32
ors3	SIRM	0.4502	83	329	w6dm3	NRM	0.0833	39	179
	impact	0.0723	78	252		impact	0.0670	19	186
ors4	SIRM	0.4830	86	34	w6dm4	NRM	0.0347	–65	69
	impact	0.1563	77	213		impact	0.0204	–54	94
ors5	SIRM	0.3828	81	347	w6dm5	NRM	0.0610	53	1
	impact	0.1007	65	355		impact	0.0644	43	77
ors6	SIRM	0.4102	8	177	w6dm6	SIRM	0.2977	23	176
	impact	0.1955	5	178		impact	0.1199	22	178
ors7	SIRM	0.4881	5	97	w6dm7	NRM	0.0603	33	142
	impact	0.2183	4	103		impact	0.0421	41	140

Kletetschka et al. 2000a). However, given the early time proposed for the origin of these anomalies (Acuña et al. 1999), this source appears to be unlikely, because the large volume of rocks that would have to be formed, eroded, deposited, and deeply buried within a relatively short time scale.

The magnetic source can consist of early oxide cumulates within the deep, initially very oxidized, igneous gabbro/norite rocks dominated by hemoilmenite (McEnroe et al. 2001b; Wilson et al. 1996) (ilmenite host with titanohematite lamellae). This requirement for oxidized gabbro/norite type of rock would indicate a widespread occurrence of early highly oxidized magma, either derived from the early highly oxidized composition of the planet or from the mixing with the early oxygen-rich fluids originating from a large body of water on the surface, possibly an early ocean on Mars. However, we have to state that our implications of high oxidation state are not supported by the analyses of martian meteorites, perhaps indicating that the meteorites came from the crustal material that originated outside the Terra Sirenum region.

CONCLUSIONS

Experimental impacts, in absence of an ambient magnetic field, achieving pressures of 0.5–2.0 Gpa, on individual, well-characterized magnetic minerals significantly demagnetize pre-existing levels of magnetization. Titanohematite preserves 75 ± 11%; SD magnetite 33 ± 8%; MD hematite 33 ± 10%; and MD magnetite 12 ± 3% of its initial magnetization after an impact. Elastic-impact magnetic resistance increases linearly with the logarithm of the magnetic coercivity. Impact demagnetization associated with the large impact basins on Mars was not sufficient to demagnetize the martian crust to large distances from the crater owing to the pressure interference zone associated with the impacts. The impact pressure analysis and distribution of magnetic sources within the depth of 100 km allow a crude correlation of magnetic anomalies with crustal magnetic coercivity. Sources near Hellas, Argyre, and Isidis impact basins are of moderate magnetic coercivity and are consistent with magnetite and/or pure hematite. Sources near the Prometheus basin possess significantly larger magnetic coercivity ruling out magnetite as a major magnetic source. Magnetite can still contribute, but less than another high- coercivity mineral. The Prometheus basin is in the proximity of Terra Sirenum, the region with intense magnetic anomalies (southern hemisphere between 142–210° W longitude). The magnetic anomaly data indicate that the source of this magnetic complex may have a different nature than the rest of the anomalies. Large magnetic coercivity requirement for this region suggests that a plausible magnetic source should consist of coarse-grained exsolved titanohematite and/or pyrrhotite in addition to magnetite. Even though currently there is no evidence for high oxidation of the martian crust, our data support that high oxidation may be occurring, at least regionally, in the Terra Sirenum region.

Acknowledgments–We used IDL code to plot the MOLA and magnetic data developed by Jim Roark (Roark and Frey 2001), available at http://core2.gsfc.nasa.gov/mola_pub/gridview. We acknowledge the contributions of Dr. Peter J. Wasilewski at GSFC/NASA who provided most of the lab equipment and space for this impact modeling study and review by B. P. Glass. We acknowledge help from Jana Just, Tomas Kohout, Michael Loweth, and Professor James Stout. We thank Sarah Stewart and one anonymous reviewer for important comments that significantly improved this paper. Research was supported by the research project ASCR No. 23013972 and grant project ASCR No. A3013406.

Editorial Handling—Dr. Elisabetta Pierazzo

REFERENCES

Acuña M. H., Connerney J. E. P., Ness N. F., Lin R. P., Mitchell D., Carlson C. W., McFadden J., Anderson K. A., Rème H., Mazelle C., Vignes D., Wasilewski P., and Cloutier P. 1999. Global distribution of crustal magnetization discovered by the Mars Global Surveyor MAG/ER experiment. *Science* 284:790–793.

Ahrens T. J. and O'Keefe J. D. 1977. Equations of state and impact-induced shock-wave interaction on the Moon. In *Impact and explosion cratering,* edited by Roddy D. J. Pepin R., and Merrill R. New York: Pergamon. pp. 639–656.

Arkani-Hamed J. 2002. Magnetization of the martian crust. *Journal of Geophysical Research* 107, doi:10.1029/2001JE001496.

Bass J. D. 1995. Elasticity of minerals, glasses, and melts. In *Mineral physics and crystallography: A handbook of physical constants.* Washington D.C.: American Geophysical Union.

Cisowski S. M. and Fuller M. 1978. Effect of shock on magnetism of terrestrial rocks. *Journal of Geophysical Research* 83:3441–3458.

Connerney J. E. P., Acuña M. H., Wasilewski P. J., Ness N. F., Rème H., Mazelle C., Vignes D., Lin R. P., Mitchell D. L., and Cloutier P. A. 1999. Magnetic lineations in the ancient crust of Mars. *Science* 284:794–798.

Connerney J. E. P., Acuña M. H., Wasilewski P. J., Kletetschka G., Ness N. F., Rème H., Lin R. P., and Mitchell D. L. 2001. The global magnetic field of Mars and implications for crustal evolution. *Geophysical Research Letters* 28:4015–4018.

Connerney J. E. P., Acuña M. H., Ness N. F., Spohn T., and Schubert G. 2004. Mars crustal magnetism. *Space Science Reviews* 1:1–33.

Frost B. R. 1991. Stability of oxide minerals in metamorphic rocks. In *Oxides minerals: Petrologic and magnetic significance,* edited by Lindsley D. H. Washington D.C.: Mineralogical Society of America. pp. 490–509.

Gilder S. A., LeGoff M., Peyronneau J., and Chervin J. 2002. Novel high pressure magnetic measurements with application to magnetite. *Geophysical Research Letters* 29, doi:10.1029/2001GL014227.

Halekas J. S., Mitchell D. L., Lin R. P., Hood L. L., Acuña M. H., and Binder A. B. 2002. Demagnetization signatures of lunar impact craters. *Geophysical Research Letters* 29, doi:10.1029/2001GL013924.

Harrison K. P. and Grimm R. E. 2002. Controls on martian hydrothermal systems: Application to valley network and magnetic anomaly formation. *Journal of Geophysical Research* 107, doi:10.1029/2001JE001616.

Hood L. L., Richmond N. C., Pierazzo E., and Rochette P. 2003. Distribution of crustal magnetic anomalies on Mars: Shock

effects of basin-forming impacts. *Geophysical Research Letters* 30, doi:10.1029/2002GL016657.

Jacquemont B. 2002. *Etude des interactions eaux-roches dans le granite de Soultz-sous-Forêts. Quantification et modélisation des transferts de matière par les fluides.* Strasbourg: Université Luis Pasteur. 130 p.

Just J., Schleicher A., Kontny A., and de Wall H. 2002. The influence of hydrothermal activity on rock magnetic properties of granites from the EPS-1 drilling (Soultz-sous-Forêts, France) (abstract #EGS02-A-04783). 27th EGS General Assembly. *Geophysical Research Abstracts* 4.

Kletetschka G. 1998. Petrogenetic grids and their application to magnetic anomalies in lower crustal rocks, Labrador. Ph.D. thesis, University of Minnesota, Minneapolis, Minnesota, USA.

Kletetschka G. and Stout J. H. 1998. The origin of magnetic anomalies in lower crustal rocks, Labrador. *Geophysical Research Letters* 25:199–202.

Kletetschka G. and Wasilewski P. J. 2002. Grain size limit for SD hematite. *Physics of the Earth and Planetary Interiors* 129: 173–179.

Kletetschka G., Wasilewski P. J., and Taylor P. T. 2000a. Hematite vs. magnetite as the signature for planetary magnetic anomalies? *Physics of the Earth and Planetary Interiors* 119:259–267.

Kletetschka G., Wasilewski P. J., and Taylor P. T. 2000b. Mineralogy of the sources for magnetic anomalies on Mars. *Meteoritics & Planetary Science* 35:895–899.

Kletetschka G., Wasilewski P. J., and Taylor P. T. 2000c. Unique thermoremanent magnetization of multidomain sized hematite: Implications for magnetic anomalies. *Earth and Planetary Science Letters* 176:469–479.

Kletetschka G., Wasilewski P. J., and Taylor P. T. 2002. The role of hematite-ilmenite solid solution in the production of magnetic anomalies in ground and satellite based data. *Tectonophysics* 347:166–177.

Kletetschka G., Ness N. F., Wasilewski P. J., Connerney J. E. P., and Acuña M. H. 2003. Possible mineral sources of magnetic anomalies on Mars. *The Leading Edge* 22:766–768.

Langlais B., Purucker M. E., and Mandea M. 2004. Crustal magnetic field of Mars. *Journal of Geophysical Research* 109, doi: 10.1029/2003JE002048.

McEnroe S. A., Harrison R. J., Robinson P., Golla U., and Jercinovic M. J. 2001a. Effect of fine-scale microstructures in titanohematite on the acquisition and stability of natural remanent magnetization in granulite facies metamorphic rocks, southwest Sweden: Implication for crustal magnetism. *Journal of Geophysical Research* 106:30,523–30,546.

McEnroe S. A., Robinson P., and Panish P. T. 2001b. Aeromagnetic anomalies, magnetic petrology, and rock magnetism of hemo-ilmenite- and magnetite-rich cumulate rocks from the Sokndal Region, South Rogaland, Norway. *American Mineralogist* 86: 1447–1468.

Melosh H. J. 1989. *Impact cratering: A geologic process.* New York: Oxford University Press. 245 p.

Milkovich S. M., Head J. W., and Pratt S. 2002. Meltback of Hesperian-aged ice-rich deposits near the south pole of Mars: Evidence for drainage channels and lakes. *Journal of Geophysical Research* 107, doi:10.1029/2001JE001802.

Mohit P. S. and Arkani-Hamed J. 2004. Impact demagnetization of the martian crust. *Icarus* 168:305–317.

Morgan J., Warner M., Brittan J., Buffler R., Camargo A., Christeson G., Denton P., Hildebrand A., Hobbs R., Macintyre H., Mackenzie G., Maguire P., Marin L., Nakamura Y., Pilkington M., Sharpton V., Snyder D., Suarez G., and Trejo A. 1997. Size and morphology of the Chicxulub impact crater. *Nature* 390:472–476.

Nagata T. 1971. Introductory notes on shock remanent magnetization and shock demagnetization of igneous rocks. *Pure and Applied Geophysics* 89:159–177.

Nimmo F. and Gilmore M. S. 2001. Constraints on the depth of magnetized crust on Mars from impact craters. *Journal of Geophysical Research* 106:12,315–12,323.

Pilkington M. and Grieve R. A. F. 1992. The geophysical signature of terrestrial impact craters. *Reviews of Geophysics* 30:161–181.

Pohl J., Bleil U., and Hornemann U. 1975. Shock magnetization and demagnetization of basalt by transient stress up to 10 Kbar. *Zeitschrift für Geophysik* 41:23–41.

Roark J. H. and Frey H. V. 2001. GRIDVIEW: Recent improvements in research and education software for exploring Mars topography (abstract #1618). 33rd Lunar and Planetary Science Conference. CD-ROM.

Robinson P., Harrison R. J., McEnroe S. A., and Hargraves R. B. 2002. Lamellar magnetism in the haematite-ilmenite series as an explanation for strong remanent magnetization. *Nature* 418:517–520.

Rochette P., Fillion G., Ballou R., Brunet F., Ouladdiaf B., and Hood L. 2003a. High pressure magnetic transition in pyrrhotite and impact demagnetization on Mars *Geophysical Research Letters* 30, doi:10.1029/2003GL017359.

Schenk P. M. and Moore J. M. 2000. Stereo topography of the south polar region of Mars: Volatile inventory and Mars polar lander landing site. *Journal of Geophysical Research* 105:24,529–24,546.

Schmidt R. M. and Housen K. R. 1987. Some recent advances in the scaling of impact and explotion cratering. *International Journal of Impact Engineering* 5:543–560.

Smith D. E., Zuber M. T., Solomon S. C., Phillips R. J., Head J. W., Garvin J. B., Banerdt W. B., Muhleman D. O., Pettengill G. H., Neumann G. A., Lemoine F. G., Abshire J. B., Aharonson O., Brown C. D., Hauck S. A., Ivanov A. B., McGovern P. J., Zwally H. J., and Duxbury T. C. 1999. The global topography of Mars and implications for surface evolution. *Science* 284:1495–1503.

Tanaka K. L. and Scott D. H. 1987. Geological map of the polar regions of Mars. Reston: U.S. Geological Survey.

Tanaka K. L., Greeley R., Scott D. H., and Guest J. E. 1986. *New geologic map of Mars.* NASA Technical Memorandum 88383. pp. 601–602.

Voorhies C. V., Sabaka T. J., and Purucker M. 2002. On magnetic spectra of Earth and Mars. *Journal of Geophysical Research* 107, doi:10.1029/2001JE001534.

Weiss B. P., Shuster D. L., and Stewart S. T. 2002a. Temperatures on Mars from $^{40}Ar/^{39}Ar$ thermochronology of ALH 84001. *Earth and Planetary Science Letters* 201:465–472.

Weiss B. P., Vali H., Baudenbacher F. J., Kirschvink J. L., Stewart S. T., and Shuster D. L. 2002b. Record of an ancient martian magnetic field in ALH 84001. *Earth and Planetary Science Letters* 201:449–463.

Wilson J. R., Robins B., Nielsen F. M., Duchesne J. C., and Auwera J. V. 1996. The Bjerkreim-Sokndal layered intrusion, Southwest Norway. In *Layered intrusions,* edited by Cawthorn R. G. Amsterdam: Elsevier Science. pp. 231–255.

Zuber M. T. 2001. The crust and mantle of Mars. *Nature* 412:220–227.